CHAPTER - 8
ELECTRON PARAMAGNETIC RESONANCE STUDY OF Gd_2O_3/NiO CORE-SHELL NANOPARTICLES

8.1 Introduction

Magnetism of small particles has generated increasing interest due to their unique physical and biological properties as well as their technological applications [1]. Bulk nickel oxide (NiO) is known to be a two-sublattice antiferromagnet with NaCl crystalline structure and Neel temperature of 523 K [2]. However, after nanostructuring into ultra small particles, the characteristics of this material become anomalous. According to Rubintein *et al*. [3], electron spin resonance (ESR) signal of 60 Å NiO NPs observed at the lowest temperature. In the case of bulk NiO particle including above 100 nm particles, the ESR signal vanish due to the emergence of large molecular exchange fields. Pishko *et al*. [4] found that the magnetic resonance in 57Å NiO showed the two separate peaks due to the size effect and it confirms the presence of many-sublattice magnetic structure leads to the additional exchange modes of magnetic resonance.

Gadolinium oxide (Gd_2O_3) is a well-known material, has been widely used for various applications such as in magnetic [5, 6], catalytic [7], phosphor [8], nuclear [9] and optical fields [10]. Ahren *et al*. [11] reported that Gd_2O_3 NPs shown a high relaxivity compared with commonly used gadolinium (III) chelates, indicating that Gd_2O_3 particles are promising for future use in MRI cell tracking and bioimaging applications. Recently, water-dispersible MnO NPs were reported as a T_1 (spin-lattice relaxation time) MRI contrast agent for body organs like brain, the liver and the kidney [12]. The efficient positive contrast agent making is very often addresses, large number of paramagnetic atoms (e.g., Gd^{3+}) within small volumes or confine the

contrast agents inside the matrix [13-18]. Gustafsson *et al*. [19] reported the Gd_2O_3 NP can serve as positive contrast agent to reduce T_1 relaxation time resulting in a brighter signal. Recent studies reveals, that the core/shell nanoparticles (CSNPs) can enter the cells and they act as efficient contrasting agent due to their better spin-lattice relaxation time [20, 21]. The intent of the present work is to discuss the subject of magnetic and spin relaxation studies of NiO encapsulated Gd_2O_3 CSNPs in the temperature range from 300 K to 110 K employing the electron spin resonance (ESR) spectroscopy at a frequency of 9.43 GHz. The ESR is a powerful technique to analyse the magnetic properties and spin dynamics in a condensed matter.

8.2 Experimental Procedure

8.2.1 Materials and Method

The reagent grade of $Gd(NO_3)_3.6H_2O$(Alfa Aesar) and $Ni(NO_3)_2.6H_2O$ (Alfa Aesar) were used as starting materials. Polyethylene glycol 400 (PEG) was used as solvent and double distilled water and ethanol were employed for washing.

For the synthesis of NiO and Gd_2O_3 NPs, 12 mM of $Ni(NO_3)_2.6H_2O$ and 12 mM of $Gd(NO_3)_3.6H_2O$ were dissolved separately in 30 ml of polyethylene glycol (PEG) under stirring in a round bottomed flask at 100 $^{\circ}$C. The clear transparent salt solutions obtained were subsequently heated to 180 $^{\circ}$C for 90 min. The resulting greenish brown solution of NiO and brown suspension of Gd_2O_3 were cooled to room temperature, diluted with ethanol and the NPs were separated from the solutions by centrifugation at 10,000 rpm. To remove unreacted precursor and PEG, the sediment materials were dispersed in ethanol and centrifuged at three times. The materials obtained after centrifugation were calcined at 600 $^{\circ}$C for 2 h in air. To get the NPs of Gd_2O_3/NiO core-shell, NiO shell was grown on the Gd_2O_3 core employing a two step process. Firstly, the as-prepared Gd_2O_3 core NPs was dispersed in 25 ml of PEG

under sonication for 10 min and then a solution of PEG (15 ml) containing 12 mM of $Ni(NO_3)_2.6H_2O$ was injected into the dispersed nanocore system. After mixing the above solution (using a magnetic stirrer for 15 min), the mixed system was heated at 180 $^{\circ}$C for 2 h and cooled to room temperature, washed, centrifuged and after that calcined at 600 $^{\circ}$C for 2 h in air to get Gd_2O_3/NiO CSNPs.

8.2.2 Characterisation Techniques

To confirm the phase formation, crystal structure and purity of the synthesised samples, diffraction pattern of the powder samples was taken by powder X-ray diffractometer (Rigaku Miniflex-II) at room temperature. TEM micrographs were obtained using a TECHNAI G^2 TF20ST transmission electron microscope operating at 200 kV. Samples for TEM were prepared by placing a drop of a colloidal acetone solution of the powder sample onto a carbon coated copper grid, and the grid was dried in air. Raman spectrum of the sample was obtained at an excitation wavelength of 488 nm using a Lab-RAM HR 800 (Jobin Yvon) Raman spectrometer. Variable temperature EPR spectra were recorded using a Bruker EMX plus spectrometer operating at X-band (ν = 9.43 GHz) with 100 kHz magnetic field modulation. The temperature was varied from 300 K to110 K and the EPR spectra were recorded while warming the sample. Magnetic characterisation of the NPs was carried out using an ADE EV9 model vibrating sample magnetometer (VSM) by applying a maximum field of 20 kOe.

8.3 Results and Discussion

8.3.1 Structural Analyses

In the XRD pattern of Gd_2O_3 core NPs, as shown in Figure 8.1a, the major peaks are obtained at 2θ = 28.50°, 33.06°, 47.44° and 56.34° and the corresponding (hkl) planes are (222), (400), (440) and (622) respectively. The nature and position of

the above diffraction peaks are characteristics of cubic Gd_2O_3 phase (JCPDS card No.: 43-1014). Typical XRD pattern of NiO NPs, as shown in Figure 8.1b, showing the existence of strong and sharp diffraction peaks at 2θ values 37.25°, 43.30° and 63.08° and the respective crystal planes are (111), (200) and (220). These peaks matched well with those reported results (JCPDS card No.: 4-0835 & [22-24]). The Gd_2O_3 and NiO diffraction patterns are observed in the Gd_2O_3/NiO core/shell nanosystem, as shown in Figure 8.1c, but its diffraction angles are slightly shifted to the higher angle from their bare one. This may be due to the strain existed in core-shell structures which are reported by Cao and Banin [25] in epitaxial growth of an InP shell on an InAs core. In the present study, shifting in the diffraction angles at higher values may be due to the very small thickness of the shell material on the core NPs. So the strain from the epitaxial growth of the shell material on the core is strongly affected and is observed as shift in the diffraction pattern of these CSNPs.

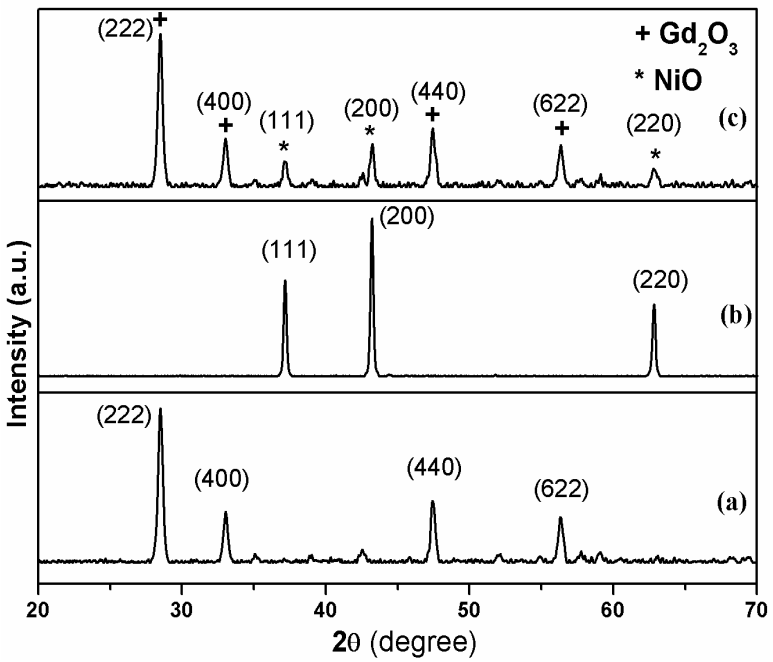

Figure 8.1 X-ray diffraction patterns obtained for (a) Gd_2O_3, (b) NiO and (c) Gd_2O_3/NiO NPs

8.3.2 Raman Studies

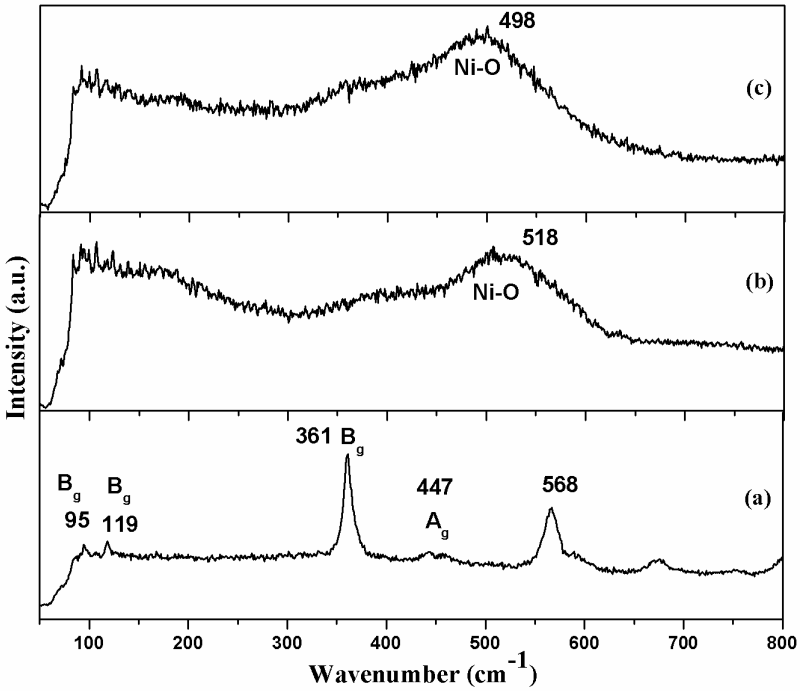

Figure 8.2 Raman spectra of (a) Gd_2O_3, (b) NiO and (c) Gd_2O_3/NiO NPs

In the Raman spectroscopy studies, pure Gd_2O_3 NPs clear peaks at 95, 119, 360 and 447 cm^{-1}, as shown in Figure 8.2a, indicate that the Gd_2O_3 NPs are in cubic phase [26]. The NiO nanoparticle (Figure 8.2b) shows broad peak at 518 cm^{-1} due to Ni-O stretching mode [27]. In the case of Gd_2O_3/NiO CSNPs (Figure 8.2c), NiO peak only observed at 498 cm^{-1}due to the presence of Ni-O stretching mode and the core material peaks are not observed, the shift in lower energy of this peak is due to the increase in the size of CSNPs and Gd_2O_3 core material peaks are found to be diminished by the mass effects of the NiO shell material [28].

8.3.3 Transmission Electron Microscopy

The TEM micrograph obtained for Gd_2O_3/NiO CSNPs is shown in Figure 8.3a. The average particle diameter is found to be around 35 nm and the structure of these particles is slightly elongated in shape. The core-shell structure can be clearly seen from the high magnification TEM micrograph (Figure 8.3b). It displays the darker

part of the Gd_2O_3 core material is encapsulated by the lighter part of NiO shell layer.

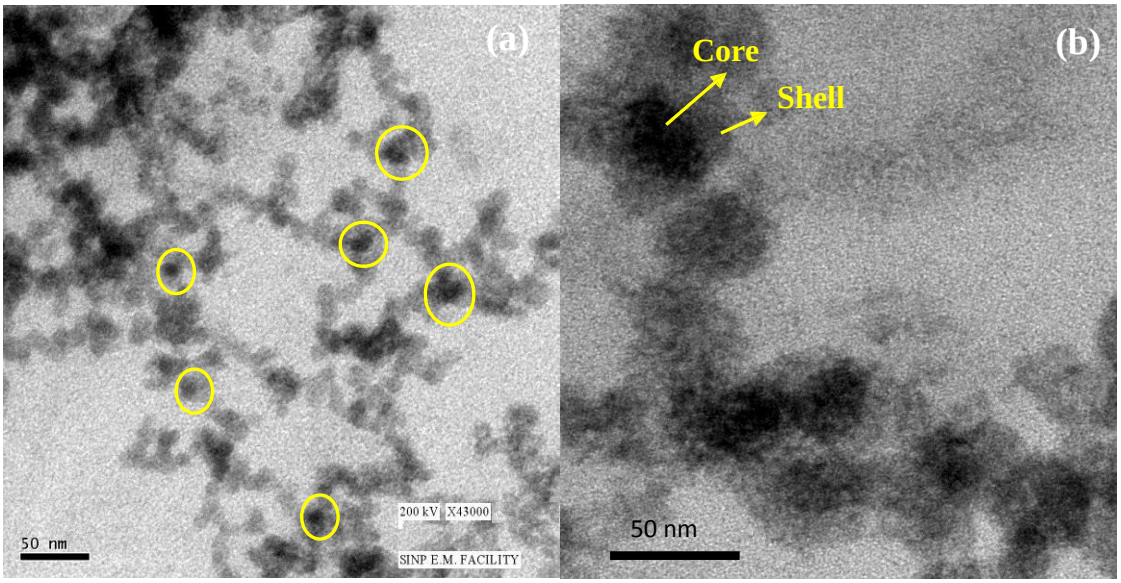

Figure 8.3 (a) TEM and (b) Higher magnification (X71,000) TEM micrograph obtained for Gd_2O_3/NiO CSNPs

8.3.4 Magnetic Characterisations

8.3.4.1 Vibrating Sample Magnetometer (VSM)

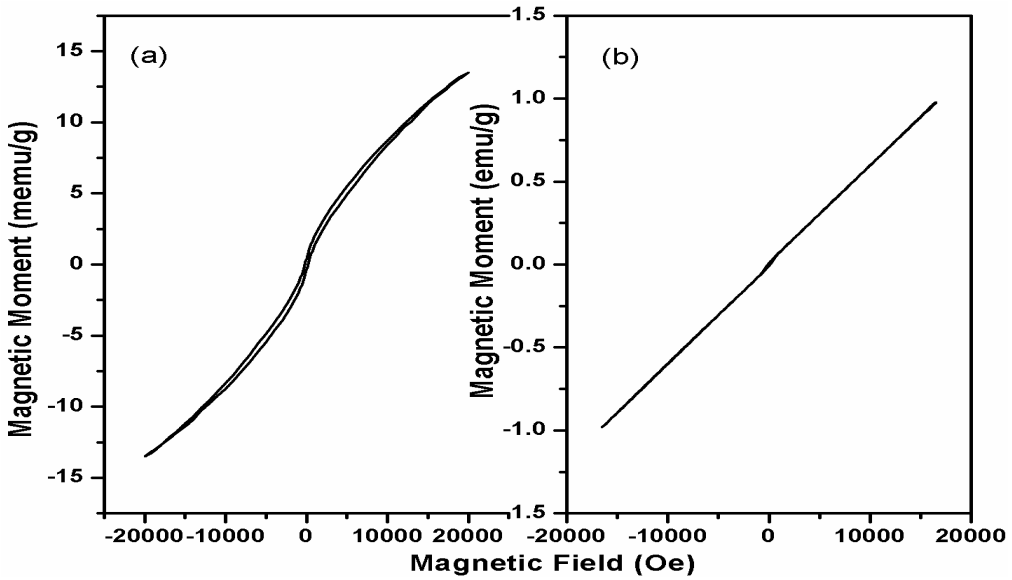

Figure 8.4 Room temperature hysteresis curves obtained for (a) NiO and (b) Gd_2O_3/NiO CSNPs

The magnetic hysteresis for the NiO and Gd_2O_3/NiO CSNPs at room temperature obtained using VSM is presented in Figure 8.4. It is observed that the magnetization of the NiO NPs (Figure 8.4a) increases rapidly with applied magnetic field and is not saturated even at 20 kOe and the value of coercivity (H_c) is found to be 187 Oe. The NiO is a typical antiferromagnetic material in the bulk form but we observed coercivity in the present case indicates the uncompensated surface spins causing a change in the magnetic order of NiO NPs [29, 30]. In the case of NiO encapsulated Gd_2O_3 CSNPs (Figure 8.4b), it reveals that the magnetization increases rapidly without reaching saturation in a field at 16 kOe and the H_c value is 85 Oe. This linear M-H behaviour is characteristics of a typical diamagnetic material. This decreased magnetic property of Gd_2O_3/NiO CSNPs may be due to the non-magnetic contribution of Gd_2O_3 core at room temperature. The observed value of the magnetic moment is very low and the H_c value is 85 Oe for the CSNPs and this may be associated with surface spins arising from the nanoscale thickness of the NiO shell material.

8.3.4.2 Electron Paramagnetic Resonance (EPR) Studies

Typical first derivative EPR spectra obtained for the Gd_2O_3/NiO CSNPs in the temperature range of 110 K to 300 K are shown in Figure 8.5. The spectra reveal a single broad signal from 300 K to 200 K. In addition to the broad signal, a small narrow signal corresponding to a resonance field (H_r) of 3940 Gauss is present when the temperature is further decreased to 150 K and 110 K respectively. The appearance of additional small signal at low temperature may be due to the anisotropy present in the sample induced by the strain in the NPs which is associated with the large surface area of the NPs [31]. When the temperature is increased, this anisotropy energy is suppressed by the thermal energy and we get the homogeneous broad signal from the

temperature range of 200 K to 300 K.

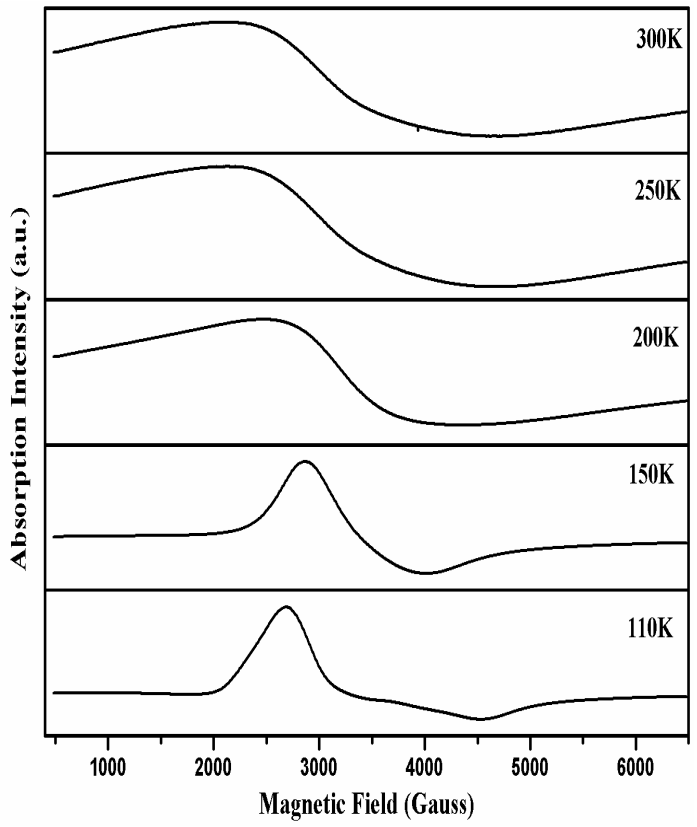

Figure 8.5 EPR spectra for Gd_2O_3/NiO CSNPs obtained at low temperatures of 300K-110K

The peak-to-peak linewidth (ΔH_{pp}) is found to increase rapidly with the increment of the temperature (Table 8.1). This is usually caused in the CSNPs by the magnetic dipole interactions at high temperatures. When the temperature is decreased, the average anisotropic field of the present sample may dominate the interparticle dipolar interaction, thus may lead to the reduction in the width producing relatively a narrow signal [32]. The ΔH_{pp} values for NiO encapsulated Gd_2O_3 NPs are larger than the reported bare Gd_2O_3 NPs at room temperature [19].

The energy between two adjacent degenerate spin energy levels, ΔE, has the same behaviour of the line width. The reduction of linewidth may cause a reduction in the separate energy ΔE. The value of ΔE is given by the relation $\Delta E=h\nu=g\mu_B H_0$ [33].

The peak-to-peak linewidth (ΔH_{pp}) and g-values are decreasing with the decrement of the temperature (Table 8.1), which depends upon two main factors namely magnetic dipole interactions among the particles and exchange interaction between the ions. Strong dipole interaction gives a large ΔH_{pp} and strong superexchange interaction produces a small ΔH_{pp} [32]. In core-shell magnetic nanosystem, interfacial exchange coupling between the core and shell region also plays as an important parameter. Ong *et al*. [34] reported that the exchange coupling between core and shell region is strong under low temperature conditions.

If the temperature is decreased, anisotropy field of the NPs and interfacial exchange coupling between core and shell region will greatly affect the ΔH_{pp} and g-values. At higher temperatures, spin direction between the antiferromagnetic NiO shell and the non-magnetic Gd_2O_3 core are different and in this condition, interfacial exchange coupling between the core and shell regions is not too significant [35]. Sunderesan *et al*. [36] found that the non-magnetic metal oxide NPs show the ferromagnetic moment because of the presence of defects on the surface of the material. In the present case at low temperature, disordered spins on the Gd_2O_3 core surface coupled with interface of shell material results in the arising of net magnetic moment from 150 K to 110 K. The interfacial roughness between the core and the shell region will be larger when the core surface disorder increases. This increasing interfacial roughness leads to a greater degree of uncompensated spin at the interface [35] and hence a larger degree of unidirectional coupling between antiferromagnetic shell (NiO) and non-magnetic core (Gd_2O_3) from 150 K in Gd_2O_3/NiO CSNPs system occurs. The g-factor value increases at 110 K which may be due to the strong interfacial exchange coupling between the core and shell region.

Table 8.1 EPR characteristics of Gd_2O_3/NiO CSNPs at different temperatures

Temperature (K)	ΔH_{pp} (Gauss)	g-value	$T_2 \times 10^{-11}$(s)	$T_1 \times 10^{-12}$(s)	Number of spin (Ns)sping^{-1}
110	1844	2.09	1.70	8.51	1.70×10^{14}
150	1151	1.98	2.87	4.51	1.11×10^{14}
200	1877	2.05	1.70	81.60	2.81×10^{13}
250	2522	2.13	1.22	12.20	2.88×10^{13}
300	2562	2.13	1.20	12.40	1.92×10^{13}

It is known that there are two relaxation processes in EPR system *viz*. spin-lattice and spin-spin relaxation. If the linewidth of the EPR spectrum is determined by spin-spin relaxation, the ΔHpp will increase rapidly as the temperature decreases [37] but we get only opposite trend in our system. Therefore, it may not be associated with the spin-spin relaxation that plays a dominant role but the other mechanism, such as spin-lattice relaxation should be operative. If the involved spins are like (parallel) the magnetic exchange interaction causes a broadening of the resonance lines, at higher temperature. On the contrary, if the magnetic exchange takes place between unlike (anti-parallel) spins a narrowing resonance lines are caused at higher temperatures. The observed broadening of the EPR peaks at higher temperatures in the present case may be attributed to the exchange interaction between the like spins. Due to the spin-lattice relaxation characteristics of Gd_2O_3/NiO CSNPs, it can be used as a T_1 contrast agent in the MRI application [20, 21]. The Homogeneous broadening and the peak-to-peak linewidth of the EPR spectra are used to estimate the spin-spin relaxation time (T_2) and spin-lattice relaxation time (T_1) [38]:

$$1/T_2 = g\mu_B\Delta H/\hbar \quad \text{..... (8.1)}$$

$$T_1 = 1/2\gamma^2 T_2 H_r^2 \text{ ..... (8.2)}$$

where, ΔH is the full-width-at-half-maximum (FWHM) of the absorption curve

($\Delta H=\sqrt{3}\Delta H_{pp}$), γ is the gyromagnetic ratio and T_1 and T_2 are calculated using Eq. (8.1) and (8.2) and the values are given in Table 8.1. The relaxation time (T_1 & T_2) estimated from the EPR studies does not show any regular trend with the temperature.

The EPR spin number is the area under the EPR absorption curve, which is proportional to the number of unpaired spins (N_s) in the sample. The EPR spin number is evaluated from the product of square of linewidth and peak to peak height (ΔH_{pp}^2 h) [39]. It is seen from the Table 8.1 that the lowest spin number (1.92×10^{13}) observed at 300 K and the spin number for both the temperature 250 K and 200 K are the same and is observed as 2.8×10^{3}. A sudden increment of EPR signal intensity is observed at 150 K and 110 K. This may be associated with the uncompensated spin arising at the interface between the core and shell region because of the fact that the exchange coupling effect at very low temperature resulted in the larger N_s value as observed for the temperature below 200 K.

8.4 Conclusions

Well-crystalline Gd_2O_3, NiO and Gd_2O_3/NiO (core/shell) NPs have been successfully synthesied by polyol process. The core-shell structures of the Gd_2O_3/NiO NPs are analysed by XRD and Raman spectroscopic studies. The average particle size of the CSNPs was found to be < 35 nm through TEM studies. The temperature dependent EPR spectra of these magnetic core-shell nanosystems were scanned from 110 K to 300 K. When temperature below 200 K, the spectra showed an additional small peak associated with the anisotropy present in the sample induced by the strain from the NPs due to the large surface area. The g-factor and N_s decreased with decreasing temperature from 300 K to 200 K and increased at very low temperatures. The results may be due to the dominance of anisotropy field and interfacial exchange coupling between the core and shell region which is usually significant at very low temperature in this NM/AFM core/shell nanosystem. Peak-to-peak line width increased with the increase of temperature indicating spin-lattice relaxation operating in these Gd_2O_3/NiO core/shell nanosystems. The electron spin relaxation time of Gd_2O_3 NPs could be changed by encapsulation of nanoscale NiO shell material.

References

1. R. W. Chantrell and K. O‟Grady, Applied magnetism, edited by R. Gerber *et al*. Kluwer Academic publishers, The Netherlands, (1994), p.113.
2. M. Trmbe, J.Phys. 12 (1951) 170.
3. M. Rubinstein, R. H. Kodama and S. A. makhlouf, J. Magn.Magn. Mater. 234 (2001) 289.
4. V. V. Pishko, S. L. Gnatchenko, V. V. Tsapenko, R. H. Kodama and Salah A. Makhlouf, J. Appl. Phys. 93 (2003) 7382.
5. J. B. Gruber, W. F. Krupte and J. M. Poindexter, J. Chem. Phy. 41 (1964) 3363.
6. N. T. McDevitt and A. D. Davison, J. Opt. Soc. Am. 56 (1966) 636.
7. J. M. Deboy and R. F. Hicks, Ind. Eng. Chem. Res. 27 (1988) 1577.
8. A. G. Murillo, C. L. Luyer, C. Dujardin, T. Martin, C. Garapon, C. Pedrini and J. Mugnier, Nucl. Instrum. Methods Phy. Res. A, 486 (2002) 181.
9. D. Balestrieri, Y. Philipponneau, G. M. Decroix, Y. Jorand and G. Hantozzi, J. Eur. ceram. Soc. 18 (1998) 1073.
10. R. M. Moon, H. R. Child, W. C. Klocher and L. J. Raubeheirner, J. Appl. Phy. 38 (1967) 1383.
11. M. Ahren, L. Selegard, A. Klasson, F. Soderlind, N.Abrikossova, C. Skoglund, T. Bengtsson, M. Engstrom, P.O. Kall and K. Uvdal, Langmuir, 26 (2010) 5753.
12. H. B. Na, J. H. Lee, K. An, Y. I. Park, M. Park, I. S. Lee, D.H. Nam, S. T. Kim, S. H. Kim, S. W. Kim, K. H. Lim, K. S. Kim, S. O. Kim and T. Hyeon, Angew. Chem. Int. Ed. 46 (2007) 5397.
13. M. A. Fortin, R. M. Petoral Jr, F. Soderlind, A. Klasson, M. Engstrom, T. Veres, P. O. Kall and K. Uvdal, Nanotechnology, 18 (2007) 395501.
14. J. L. Bridot, A. C. Faure, S. Laurent, C. Riviere, C. Billotey, B. Hiba, M. Janier, V. Josserand, J. L. Coll, L. V. Elst, R. Muller, S. Roux, P. Perriat and O. Tillement, J. Am. Chem. Soc. 129 (2007) 5076.
15. F. Evanics, P. R. Diamente, F. C. J. M. Van Veggel, G. J. Stanisz and R. S. Prosser, Chem. Mater. 18 (2006) 2499.
16. H. Hifumi, S. Yamaoka, A. Tanimoto, D. Citterio and K. Suzuki, J. Am. Chem. Soc. 128 (2006) 15090.
17. B. H. Bin Na, I. C. Song and T. Hyeon, Adv. Mater. 21 (2009) 2133.

18. H. Bin Na and T. Hyeon, J. Mater. Chem. 19 (2009) 6267.
19. H. Gustafsson, M. Ahren, F. Soderlind, J. M. C. Gallego, P. O. Kall, P. Nordblad, P. O. Westlund, K. Uvdal and M. Engstrom, J. Phys. Chem. C, 115 (2011) 5469.
20. M. Chu, X. Song, D. Cheng, S. Liu and J. Zhu, Nanotechnology, 17 (2006) 3268.
21. W. Fu, H. Yanga, Q. Yua, J. Xua, X. Panga and G. Zou, Mat. Lett. 61 (2007) 2187.
22. D. Tao and F. Wei, Mater. Lett. 58 (2004) 3226.
23. H. Guan, C. Shao, S. Wen, B. Chen, J. Gong and X. Yang, Inorg. Chem. Commun. 6 (2003) 1302.
24. H. Jiao, Nano-Micro Lett. 3 (2011)166.
25. Y. W. Cao and U. Banin, J. Am. Chem. Soc. 122 (2000) 9692.
26. C. Le Luyer, A. Garcia Murillo, E.bernstein and J.Mugnier, J. Raman Spectrosc. 34 (2003) 234.
27. S. I. C. Torresi, A. H. L. Goff and S. Joiret, J. Electrochem. Soc. 138 (1991) 1554.
28. E. B. Santos, J. M. de Souza e Silva and I. O. Mazali, Vib Spectrosc. 54 (2010) 89.
29. R. H. Kodama, S. A. Makhlouf and A. E. Berkowitz, Phys. Rev. Lett. 79 (1997) 1393.
30. M. Ghosh, K. Biswa, A. Sundaresen and C. N. R. Rao, J. Mater. Chem. 16 (2006) 106.
31. V. Tsurkan, M. Lohmann, H. A. Krug-von-Nidda, A. Loidi, S. Horn and R. Tidecks, Phys. Rev. B, 63 (2001) 125209.
32. L. Li, G. Li, R. L. Smith and H. Inomata, Chem. Mater. 12 (2000) 3705.
33. J. F. Raber, Experimental Methods in Polymer Chemistry-Physical Principal And Applications, Wiley, Newyork, (1980).
34. Q. K. Ong, A. Wei and X.M. Lin, Phys. Rev B, 80 (2009) 134418.
35. R. F. L. Evans, D. Bate and R. W. Chantrell, Phys. Rev. B, 84 (2011) 092404.
36. A. Sundaresan, R. Bhargavi, N. Rangarajan, U. Siddesh and C. N. R. Rao, Phys. Rev. B, 74 (2006) 161306(R).
37. G. Dixit, J. P. Singh, R. C. Srivastava and H. M. Agarwal, J. Magn. Magn.

Mater. 324 (2012) 479.

38. J. P. Singh, R. C. Srivastava, H. M. Agarwal, R. P. S. Kushwaha, P. Chand and R. Kumar Int. J. Nanosci. 7, (2008) 21.
39. K. H. Wu, Y. C. Chang, H. B. Chen, C. C. Yang and O. N. Horng, J. Magn. Magn. Mater. 278 (2004) 156.